Journal of Computational Acoustics, Vol. 4, No. 3 (1996) 273–290

ESTIMATING GEOACOUSTIC BOTTOM PROPERTIES FROM TOWED ARRAY DATA

S. M. JESUS
UCEH – Universidade do Algarve, Campus de Gambelas, PT-8000 Faro, Portugal

A. CAITI
DIST – Universitá di Génova, Via Opera Pia 13, IT-16145 Génova, Itália

Received 27 April 1995
Revised 16 October 1995

Estimating the seabottom geophysical structure from the analysis of acoustic returns of an explosive source (air-gun, sparker,...) has been used for a longtime as a routine survey technique. Recent work showed the possibility of using well-suited numerical models to invert the acoustic field for estimating detailed geoacoustic sediment properties. Common implementations used long synthetic aperture arrays (up to 2 km and more) in order to resolve potential environmental ambiguities of the acoustic field. Others, used vertical arrays of sensors covering a significant part of the water column to identify the channel normal mode structure and thus gather information for the bottom physical relevant properties. This paper investigates, with simulated data, the concept of using a moderate aperture physical line array and a sound source simultaneously towed by a single ship for inverting the bottom geoacoustic structure from the acoustic returns received on the array. First, bottom parameter estimators are derived and their system sensitivity is investigated. In particular, it is shown that such a system may be used to sense compressional and shear velocities on the bottom first layers. Density and attenuations (both compressional and shear) have in general small influence on the acoustic field structure and are therefore difficult to estimate. Increasing the signal frequency bandwidth by incoherent module averaging has no significant influence on sensitivity. Mismatch cases, mainly those related to array/source relative position, showed that deviations of more than $\lambda/3$ in range and $\lambda/5$ in depth may give erroneous extremum location and therefore biased final estimates. Second, two bottom parameter estimators are compared and their performance tested on a typical shallow water environment. In order to solve the underlying multiparameter inverse problem, global search optimization is used. In particular, it is shown that the use of an adaptive genetic algorithm may, in conjunction with a well-suited maximum likelihood based parameter estimator, rapidly converge to the surface extremum. Inversion results are in agreement with the predictions obtained from the sensitivity study. The mean relative error at 10 dB signal-to-noise ratio is within 1% for the compressional velocity, while greater errors are reported for the shear velocity. Comparison with recent results obtained with a radial basis functions (RBF) inversion strategy showed similar performance. Finally, results obtained with a 156 m aperture towed array showed a good agreement between the inverted compressional velocities and the ground truth measurements.

This work was supported by the Marine Science and Technology (MAST 2) Program of the European Community under contract MAS2-CT920022

1. Introduction

In the last years there has been an intense, and still growing, requirement for the usage of numeric propagation models on underwater acoustics. This demand is mainly due both to the increase on modeling capabilities of available codes and to the decrease on computation power cost. The availability of an accurate forward numerical model, allows, in principle, the inversion of the acoustic field for the environmental parameters,[1–3] source position,[4–6] source signal deconvolution[7] and receiver calibration.[8] These studies have revealed a number of new research topics such as Ocean Acoustical Tomography (OAT)[1–3] and Matched Field Processing (MFP).[9] Seabottom parameter estimation by acoustic remote sensing is also evolving from classical profiling techniques (sparker/air-gun) to complete physical model identification by applying methods that closely follow MFP and OAT. Given the numerical model prediction for each environmental parameter set, identifying real bottom parameters constrained to the array acoustic measurements, is known to be an ill-conditioned inversion problem which analytical solution is unknown. Ill-conditioning strongly depends on the nonlinearity of the function to be inverted[10] and on the dimension of the parameter search space. Brute force inversion, by extensive forward modeling exploration of the whole search space, has been widely used on matched-field processing for source localization. Using this approach for geoacoustic data inversion would be computer time prohibitive due to the high dimension of the parameter space to be searched. Therefore, the alternative taken by several authors combines a matched-field type of technique, which output is a multidimensional ambiguity surface, and powerful search algorithms that allow a quicker convergence to the extremum of that surface.[11–15]

Previous studies used either a fixed source and a vertical array or a sound source being towed away from a single receiver in order to create a synthetic aperture and resolve mode arrivals.[16–17] In principle, a shipborn only system would allow easier deployment and lower cost for surveillance of large areas. The present work is part of a larger project devoted to the development of a system where the ship is towing both the source and the array, such that the source-receiver range is constant. Such a system should specifically be designed for shallow water applications.

In particular, the present study is devoted to the investigation of the system limitations (array aperture, source frequency, etc.) and of the global search algorithms performance. In order to obtain an idea of the expected performance of the system and draw some conclusions on its operation, this study presents the objective function sensitivity to variations of: array length, source depth, receiver depth, source range, sensor noise, source frequency and frequency band. The canonical case consists of a 64 hydrophone — 4 m spacing towed array at 100 m depth and an harmonic 100 Hz source also at 100 m depth and at 200 m range. Inversion results are presented using a modified genetic algorithm (GA) based scheme that provides geoacoustic parameter estimates of compressional and shear velocities on a typical shallow water environment. An example of field data inversion with a 156 m aperture towed array concludes this study.

2. Theoretical Background

2.1. *The data model*

The deterministic sound pressure at the receiver location r_l, z_l is modeled as the solution of the wave equation for a narrowband point source exciting a horizontally stratified range-independent environment, that is the Green's function inverse zero-order Hankel transform

$$p_l(\omega_k, r_l, z_l, z_0; \gamma) = \int_0^\infty g(\kappa, \omega_k; \theta_l, \gamma, z_0) J_0(\kappa r_l) \kappa d\kappa \,, \tag{1}$$

where l denotes the lth array sensor, ω_k is the kth frequency bin, z_0 is the source depth and γ is a vector containing all the pertinent environmental parameters under estimation. Thus, at time snapshot n the L sensor array received acoustic pressure can be modeled as a multivariate complex normally distributed random variable

$$\mathbf{y}_n(\omega_k, \gamma_T) = b_n(\omega_k)\mathbf{p}(\omega_k, \gamma_T) + \boldsymbol{\varepsilon}_n(\omega_k) \,, \quad k = 1, \ldots, K \tag{2}$$

where $\boldsymbol{\varepsilon}$ is the sensor noise assumed to be zero mean and uncorrelated both in time and from sensor to sensor. The scalar b_n is a complex random variable $N(0, \sigma_b^2)$ that accounts for the nondeterministic amplitude variation at the receiver due to the environmental inhomogenities and fluctuations that are not included in the sensor noise. Subscript $_T$ denotes the true value of the environmental parameter under estimation.

2.2. *The broadband conventional matched-filter*

Function (1) being known for each given γ, the problem is to detect a known signal $\mathbf{p}(\omega_k, \gamma)$ in white noise which optimal solution is given by the well-known matched-filter. Let

$$\Phi_{\mathrm{CMF}}(\omega_k, \gamma) = |\mathbf{y}(\omega_k, \gamma_T)^H \mathbf{p}(\omega_k, \gamma)|^2 \,, \quad \gamma \in \Gamma \tag{3}$$

be the matched-filter output based on model replica prediction $\mathbf{p}(\omega_k, \gamma)$ for search parameter γ with Γ denoting the whole environmental parameter search space. Thus, the broadband optimal estimator $\hat{\gamma}_T$ of γ_T, given the model structure (1)–(2) is

$$\hat{\gamma}_T^{\mathrm{CMF}} = \arg \max_\gamma \frac{1}{K} \sum_{k=1}^{K} |\sigma_s^2(\omega_k)|^2 \Phi_{\mathrm{CMF}}(\omega_k, \gamma) \,, \tag{4}$$

where $\sigma_s^2(\omega_k)$ is the source power at frequency ω_k.

2.3. *Correlation of directional data*

A common problem encountered when analysing geoacoustic data is the superposition of the direct path source arrival with the bottom reflected data of interest. Since only the bottom reflected arrivals are of interest for inversion purpose, a possibility for separating those arrivals is by analysing the data in the wave number space domain and filter out the direct path arrival.[11] For an horizontal line array, the arrivals associated with the steepest vertical angles, which are those that have a stronger interaction with the bottom,

correspond to those arriving closer to broadside. That approach implies a transformation of the acoustic data from the hydrophone space to the wave number space which in some sense is expressed by the Green's function expression. In practice, since the acoustic pressure is a discrete function defined over a finite array aperture, it implies that an estimate of the predicted Green's function can be given by

$$\hat{g}_p(k_j, \omega, \gamma) = \frac{e^{i\pi/4}}{\sqrt{2\pi k_j}} \sum_{l=1}^{L} p_l(\omega, \gamma) e^{-ik_j r_l} \sqrt{r_l}, \quad j = 1, \ldots, N_w \tag{5}$$

where the discretization over the wave number space has been arbitrarily performed over N_w equally spaced points in $[0, 2\pi/d]$, d being the array sensor spacing (assumed constant). A one-to-one mapping from the wave number to the bearing space may be performed using $k_j = (2\pi f/c)\cos(\theta_j + \pi/2)$ for $\theta_j \in [-90°, +90°]$. With that definition $-90°$ direction is aft (towards the source) and $+90°$ is endfire. A similar expression to (5) may be used for the received data Green's function at time-snapshot n giving $\hat{g}_{y,n}(k_j, \omega, \gamma_T)$. Obviously, when computing (5) there is a windowing spatial effect that actually reduces the array resolution. Based on (5) and once a given bearing sector $\theta_j \in [\theta_l, \theta_h]$ has been selected a possible objective function can be defined as

$$\Phi_{\text{WS-CMF}}(\omega_k, \gamma) = \left| \sum_{j=j_l}^{j_h} \hat{g}_y^*(\theta_j, \omega_k, \gamma_T) \hat{g}_p(\theta_j, \omega_k, \gamma) \right|^2, \tag{6}$$

and an incoherent broadband function can be defined as the average of (6) over the required frequency band as

$$\Phi_{\text{WS-CMF}}(\gamma) = \frac{1}{k_h - k_l + 1} \sum_{k=k_l}^{k_h} \Phi_{\text{WS-CMF}}(\omega_k, \gamma), \tag{7}$$

giving a final parameter estimate

$$\hat{\gamma}_T^{\text{WS-CMF}} = \arg \max_{\gamma} \Phi_{\text{WS-CMF}}(\gamma). \tag{8}$$

Expression (6) has been written as time independent for a question of generality, where in practice it is time-snapshot dependent. In practice, time averaging is often performed over a "reasonable" time window on which the acoustic field is assumed to be stationary.

2.4. *Broadband maximum-likelihood matched-field*

Given data model (2) and assuming that the sensor noise power is constant and equal to σ_ε^2, at time snapshot n, the observation vector is normally distributed with mean $b_n(\omega_k)\mathbf{p}(\omega_k, \gamma_T)$ and covariance $\sigma_\varepsilon^2\mathbf{I}$. The problem can be stated as to determine the "best estimator", $\hat{\gamma}_T$, of γ_T given the data set $\{\mathbf{y}_n(\omega_k); n = 1, \ldots, N; k = 1, \ldots, K\}$. Thus, introducing a condensed notation grouping all K narrow frequencies on a single broadband vector, at time snapshot n, $\mathbf{Y}^n = [\mathbf{y}_n^T(\omega_1), \mathbf{y}_n^T(\omega_2), \ldots, \mathbf{y}_n^T(\omega_K)]^T$, the data set is formed

by $\{\mathbf{Y}^n;\, n = 1, \ldots, N\}$. If the time interval T used for calculating each individual Fourier transform is such that $T \gg \tau_0$ where τ_0 is the correlation time of the most coherent signal or noise, the vector $\mathbf{Y}^n$ has a near-block-diagonal covariance matrix because the Fourier coefficients at different frequencies are asymptotically uncorrelated. Independently from the nature of the assumed data model the log-likelihood function is given by

$$L(Y) = -\sum_{n=1}^{N} [(\mathbf{Y}^n - \boldsymbol{\mu}^n)^H \mathbf{R}_n^{-1} (\mathbf{Y}^n - \boldsymbol{\mu}^n) + \log \det(\pi \mathbf{R}_n)]\,, \tag{9}$$

where superscript ^{H} denotes Hilbert transpose, $\boldsymbol{\mu}^n = E[\mathbf{Y}^n]$ and $\mathbf{R}_n = \mathrm{COV}[\mathbf{Y}^n]$ which is, with the assumptions above, a diagonal matrix. Plugging the mean and covariance expressions into (9) one easily obtains

$$L(Y) = -\sum_{n=1}^{N} \sum_{k=1}^{K} \left\{ \frac{1}{\sigma_\varepsilon^2(\omega_k)} \|\mathbf{y}_n(\omega_k) - b_n(\omega_k)\mathbf{p}(\omega_k, \gamma_T)\|^2 - L \log[\pi \sigma_\varepsilon^2(\omega_k)] \right\}. \tag{10}$$

Since $\mathbf{p}(\omega_k, \gamma_T)$ is given by the model, for the search parameter γ, as $\mathbf{p}(\omega_k, \gamma)$, the only unknown is the random component $b_n(\omega_k)$. An usual assumption is to introduce a least-squares estimate of the signal, which in that case is given simply by the projection of $\mathbf{y}_n(\omega_k)$ onto the vector $\mathbf{p}(\omega_k, \gamma)$ as

$$\hat{b}_n(\omega_k) = \frac{\mathbf{p}(\omega_k, \gamma)^H \mathbf{y}_n(\omega_k)}{\|\mathbf{p}(\omega_k, \gamma)\|^2}\,. \tag{11}$$

Thus, introducing (11) into (10) one gets the estimator expression

$$\hat{\gamma}_T^{\mathrm{BBML}} = \arg \min_{\gamma} \sum_{n=1}^{N} \sum_{k=1}^{K} \left\{ \frac{1}{\sigma_\varepsilon^2(\omega_k)} \|\mathbf{y}_n(\omega_k) - \frac{\mathbf{p}(\omega_k, \gamma)^H \mathbf{y}_n(\omega_k)}{\|\mathbf{p}(\omega_k, \gamma)\|^2} \mathbf{p}(\omega_k, \gamma)\|^2 \right\}, \tag{12}$$

and after some straightforward manipulations, and noting that the only n snapshot dependent quantities are the observation vectors $\mathbf{y}_n(\omega_k)$, one can rewrite (12) as

$$\hat{\gamma}_T^{\mathrm{BBML}} = \arg \min_{\gamma} \sum_{k=1}^{K} \frac{K}{\sigma_\varepsilon^2(\omega_k)} \mathrm{tr} \left\{ \left[\mathbf{I} - \frac{\mathbf{p}(\omega_k, \gamma)\mathbf{p}(\omega_k, \gamma)^H}{\|\mathbf{p}(\omega_k, \gamma)\|^2} \right] \hat{\mathbf{R}}(\omega_k) \right\}, \tag{13}$$

where the matrix $\hat{\mathbf{R}}(\omega_k)$ is the data sample covariance matrix estimate at frequency ω_k given by the time snapshot average of the data outer products. The only unknown quantity is the noise power over the required frequency band, $\sigma_\varepsilon^2(\omega_k)$; $k = 1, \ldots, K$. Assuming a flat noise, i.e., corresponding to white noise, the noise power can be assumed constant over the frequency band and pulled out from the summation in (13).

3. Simulation Results

3.1. *Parameter sensitivity study*

The environment used in the simulation study is shown in Table 1. It is formed by an homogeneous 140 m depth water layer, above a relatively soft bottom formed by two 5 m

Table 1. Canonical environment.

Depth (m)	P vel. (m/s)	S vel. (m/s)	P att. (dB/λ)	S att. (dB/λ)	Dens. (g/cm^3)
0.0	1500	0.0	0.0	0.0	1
140.0	1550	130.0	0.1	1.7	1.49
145.0	1700	350.0	0.8	2.0	1.88
150.0	2500	900.0	0.01	0.01	2.4

thick layers and a hard halfspace at 150 m depth. A computer code based on SAFARI-FIPP[18] has been developed to implement the objective functions defined in Chapter 2 and necessary looping for searching all the environmental parameters. The system scenario includes a 64 hydrophone at 4 m spacing array with a 100 Hz sound source both at 100 m depth and at 200 m range. Testing has been performed mostly with the conventional matched-filter approach and in some cases comparisons have been made with the other objective functions (WS-CMF and BBML). The signal-to-noise ratio was computed according to

$$\mathrm{SNR}_{\mathrm{dB}} = 10 \log_{10} \frac{\sigma_b^2/(k_2 - k_1 + 1) \sum_{k=k_1}^{k_2} |\mathbf{p}(\omega_k, \gamma_T)|^2}{\sigma_\varepsilon^2}. \tag{14}$$

3.1.1. *Array aperture*

Varying the array aperture from 63 m up to 2016 m produces an increase on bottom parameters sensitivity. This increase is very steep for array apertures smaller than 250 m and then there is a saturation effect where a further increase of aperture does not give any substantial sensitivity gain (Fig. 1). This behavior tends to demonstrate that bottom parameters, such as compressional and shear velocities, can be easily sensed with moderate aperture towed arrays with a relatively small loss from the results that could be obtained with larger arrays.

3.1.2. *Frequency*

Varying source frequency between 25 and 200 Hz changes the angle of incidence and signal penetration into the bottom. An increase of frequency ameliorates the sensitivity to compressional parameters although that amelioration vanishes at deeper layers where lower frequencies gave better results. Shear parameters showed a higher sensitivity at lower frequencies, that provided also smoother curves (less minima/maxima) and, in principle, a higher potential for unambiguous inversion.

3.1.3. *Bandwidth*

Varying the source bandwidth between 2 and 60 Hz showed that there is no significant increase on sensitivity with, however, a higher smoothness of the objective function at

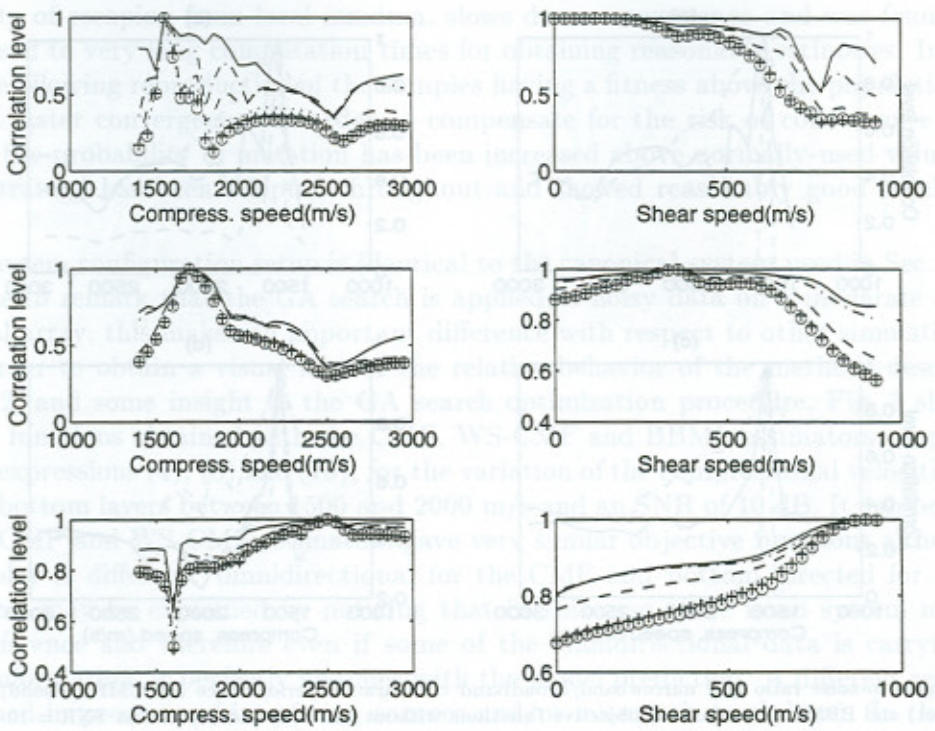

Fig. 1. Array aperture test with the CMF function for compressional and shear velocity profiles. First bottom layer on the top and deepest layer on the bottom. Array apertures of: 63 m (– solid), 126 m (-.- dash-dot), 252 m (- - - dashed), 504 m (.... dotted), 1008 m (+++) and 2016 m (o o o).

the expense of a much larger computational effort. Some broadband results are shown in Fig. 2.

3.1.4. *Source-receiver positions*

Changing relative source-receiver depth changes the sensitivity according to the higher or lower transfer of energy between source and receiver which depends on the mode excitation vs depth. That is highly dependent on the particular environment chosen for testing. Changing source receiver range has a similar behavior depending on the modal interference pattern versus range. In both cases, placing the source and the array at high energy transfer locations improves sensitivity.[19]

3.1.5. *System parameters mismatch*

As expected, a higher dependence to depth than to range mismatch was found. The accuracy to which sensor depth should be known has to be better than $\lambda/5$ while an accuracy of $\lambda/3$ will be enough for sensor range.

3.1.6. *Signal-to-noise ratio*

The narrowband and broadband performance of the algorithms has been compared and the results are shown in Fig. 2. Due to the source receiver proximity, the signal to noise ratio

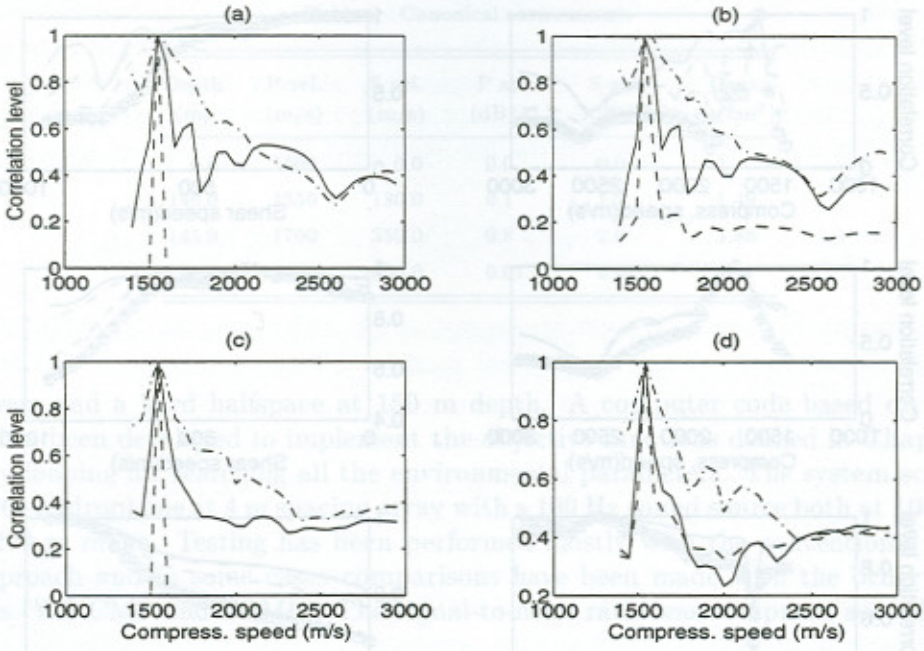

Fig. 2. Signal-to-noise ratio and narrowband/broadband comparative performance for CMF (– solid), WS-CMF (-.- dash-dot) and BBML (- - - dashed) objective functions without noise (a) and (c) and at SNR = 10 dB (b) and (d); narrowband (100 Hz) in (a) and (b) and 80–120 Hz bandwidth in (c) and (d).

(SNR) is expected to be relatively high therefore only the SNR = ∞, in (a) and (c), and 10 dB, in (b) and (d), are shown. In both the broadband and narrowband cases, the BBML estimator provided the better defined maxima at SNR = ∞. In turn, at SNR = 10 dB all estimators showed similar performance. Continuing testing at lower SNR's (not shown) CMF showed to be the most robust keeping a constant performance down to −5 dB.

3.2. *Genetic algorithm inversion*

The inversion of a highly nonlinear expression such as that relating the bottom physical parameters and the acoustic data pressure on a complex shallow water environment requires the optimization of a multidimensional ambiguity surface. The shape of the surface is, in general, virtually unknown but suspected to have several local maxima, thus inhibiting the use of classical gradient based search methods. Brute force inversion by forward search is a computationally very intensive task due to the dimensionality of the search space involved. Global search techniques being able both to avoid the exhaustive search of the whole space and to escape from local maxima are useful in such problems. Among others, the so called Genetic Algorithms (GA), have been used for this purpose and demonstrated significant potential.[13] The scope of the present paper is to concentrate on the application rather than on the GA itself. The implementation used very closely follows that proposed in Ref. 20, except for the selection of the "new" population at each iteration. The basic algorithm described in Ref. 20 forms a "roulette" based scheme where each sample of the "old" population has a chance of reproduction. This procedure, although maintaining a high

probability of escaping from local maxima, slows down convergence and was found in our case, to lead to very long computation times for obtaining reasonable estimates. Instead, a procedure allowing reproduction of the samples having a fitness above the population mean ensures a faster convergence. In order to compensate for the risk of convergence to local maxima, the probability of mutation has been increased above normally-used values. This general strategy has been adopted throughout and showed reasonably good results in all tests.

The system configuration setup is identical to the canonical system used in Sec. 3.1. We would like to remark that the GA search is applied to noisy data on a moderate aperture horizontal array; this makes an important difference with respect to other simulative studies. In order to obtain a visual idea of the relative behavior of the methods described in Chapter 2, and some insight to the GA search optimization procedure, Fig. 3 shows the objective functions obtained with the CMF, WS-CMF and BBML estimators, respectively given by expressions (4), (8) and (13), for the variation of the compressional velocities of the first two bottom layers between 1500 and 2000 m/s and an SNR of 10 dB. It can be noticed that the CMF and WS-CMF estimators gave very similar objective functions although the data in play is different: omnidirectional for the CMF and bottom directed for the WS-CMF. This may be explained by noticing that in this case there is no system mismatch nor interference and therefore even if some of the omnidirectional data is carrying little bottom information, it perfectly matches with the model prediction. A different result may be obtained in presence of interfering sources and/or mismatch (real data). In the sequel, we will concentrate on the CMF and BBML estimators. In order to better evaluate the convergence of the GA, Figs. 4 and 5 respectively show the population surface distribution for the CMF and BBML estimators along iterations 0, 1, 2 and 3.

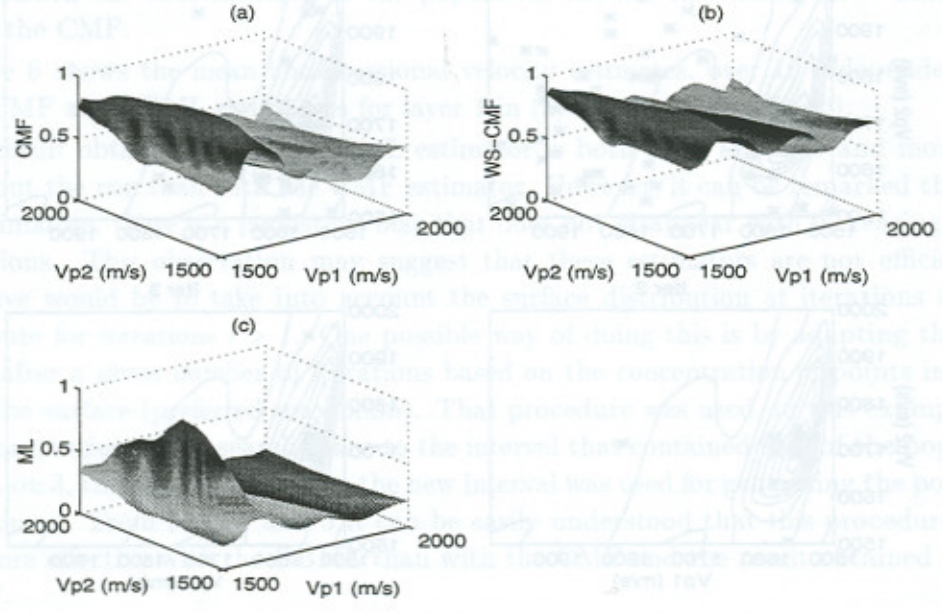

Fig. 3. Ambiguity surfaces with the canonical system configuration for the first and second layer compressional velocities between 1500 and 2000 m/s for the CMF in (a), WS-CMF with $\kappa \in [0.2, 0.45]$ in (b) and BBML in (c).

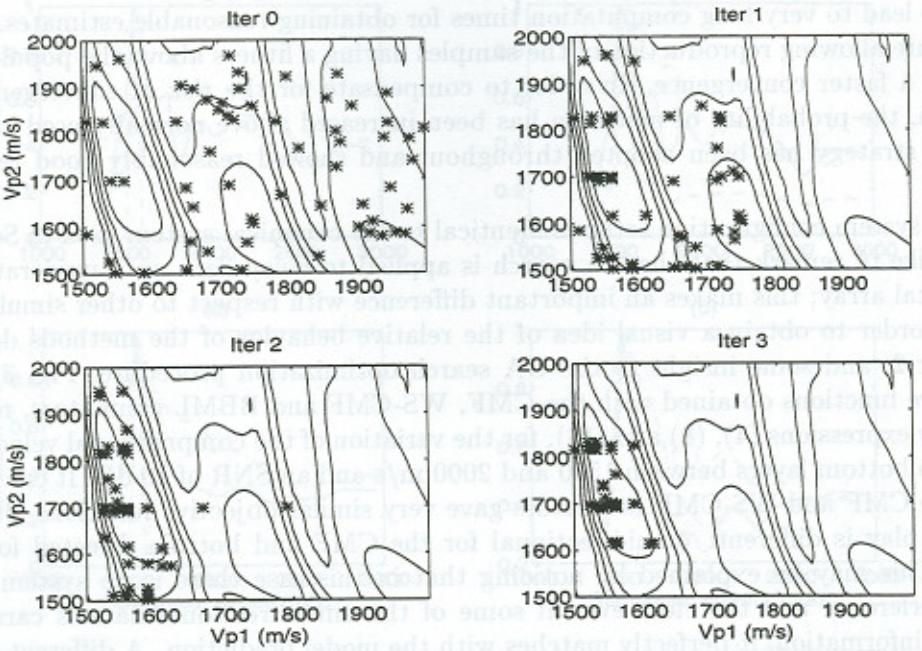

Fig. 4. GA population distribution for the CMF objective function at SNR = 10 dB and iteration number 0, 1, 2, and 3.

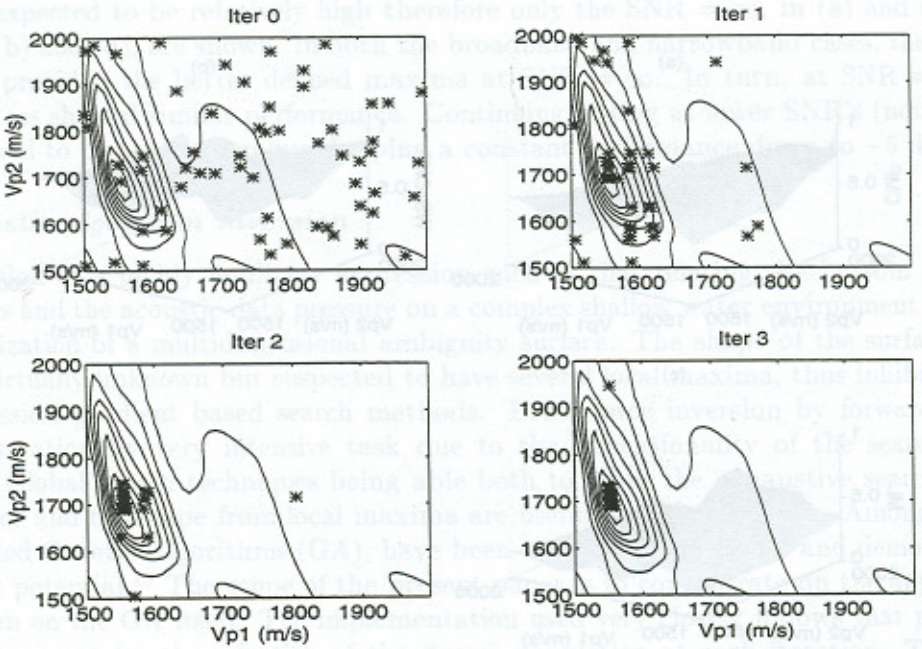

Fig. 5. GA population distribution for the BBML objective function at SNR = 10 dB and iteration number 0, 1, 2 and 3.

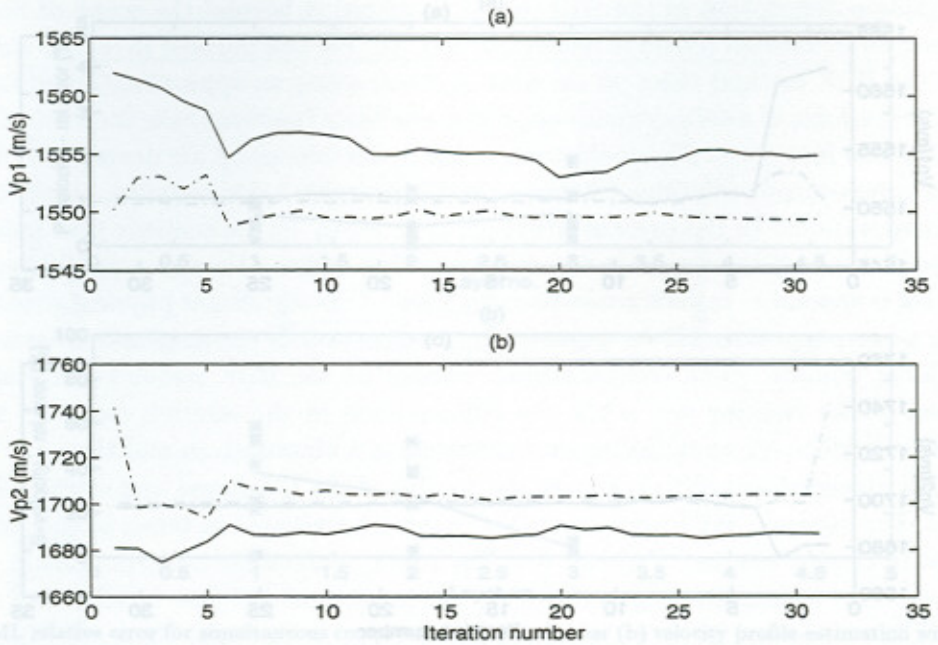

Fig. 6. Compressional velocity estimate in (m/s) versus iteration number for layer 1 in (a) and layer 2 in (b): CMF solid (–) and BBML (-.-) dashdot.

The population size has been set to 60 and mutation and crossing probabilities respectively set to 0.133 and 0.9. In this case, by comparing Figs. 4 and 5, it can be noticed that for the BBML the concentration of the population around the maximum is much faster than for the CMF.

Figure 6 shows the mean compressional velocity estimates, over 10 independent runs, for the CMF and BBML estimators for layer 1 in (a) and for layer 2 in (b).

The result obtained with the BBML estimator is both more accurate and more stable throughout the run than with the CMF estimator. However, it can be remarked that, with both estimators, there is a persistent bias that does not disappear with increasing number of iterations. This observation may suggest that these estimators are not efficient. An alternative would be to take into account the surface distribution at iterations $i \leq I$ to redistribute for iterations $i > I$. One possible way of doing this is by adapting the search interval after a given number of iterations based on the concentration of points in a given area of the surface (preferred maximum). That procedure was used, in this example, after 3 iterations, reducing the search space to the interval that contained 95% of the population. At iteration 3, the population within the new interval was used for generating the population at iteration 4. From Figs. 4 and 5 it can be easily understood that this procedure will be much more effective with the BBML than with the CMF and the result obtained is shown in Fig. 7.

The results of simultaneous inversion of the compressional and the shear velocity profiles (6 parameters) obtained with the BBML estimator are given in Fig. 8.

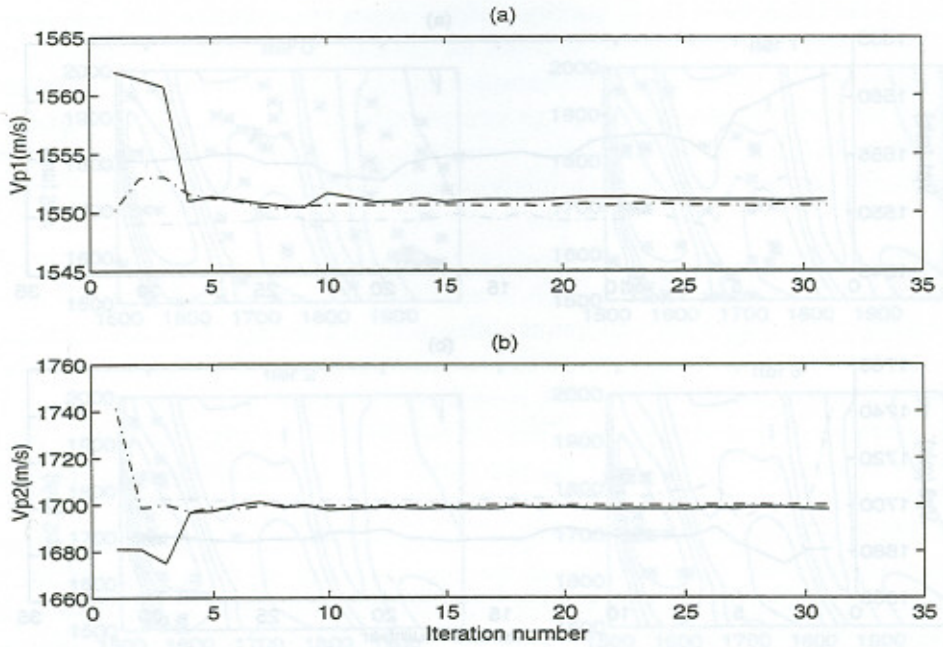

Fig. 7. Compressional velocity estimate in (m/s) versus iteration number with interval reduction after iteration 3 for layer 1 in (a) and layer 2 in (b): CMF solid (–) and BBML (-.-) dashdot.

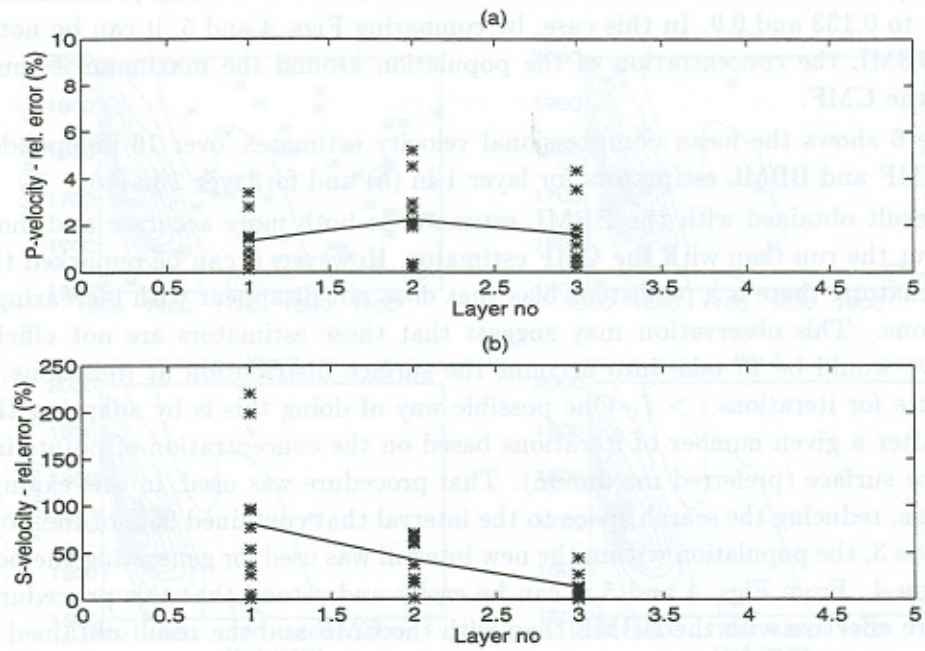

Fig. 8. BBML relative error for simultaneous compressional (a) and shear (b) velocity profile estimation. Each * represents the result of a single run and the solid line is the mean relative error computed over 10 independent runs.

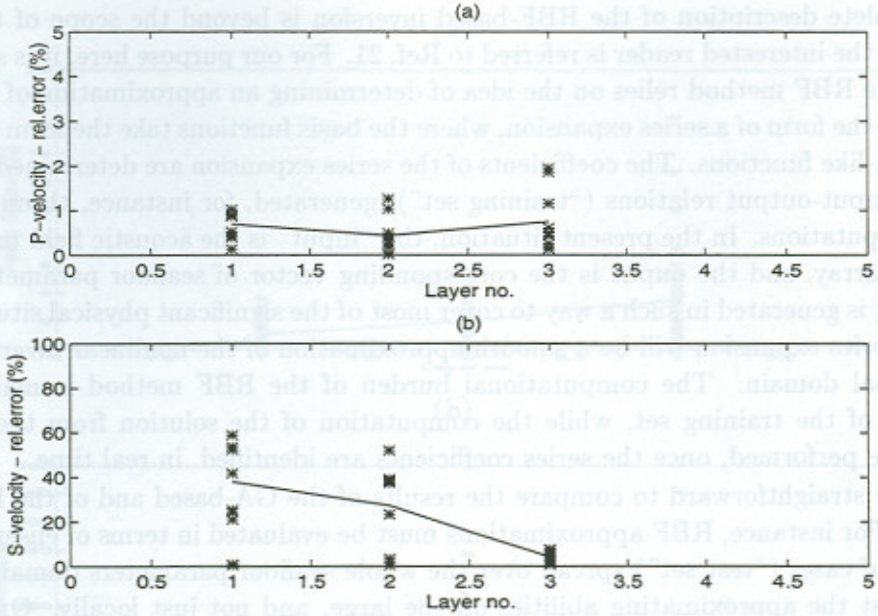

Fig. 9. BBML relative error for simultaneous compressional (a) and shear (b) velocity profile estimation with interval reduction at iterations 10 and 20. Each * represents the result of a single run and the solid line is the mean relative error computed over 10 independent runs.

This example shows that the differences of sensitivity of the objective function to compressional and shear velocities results, in this example, in a compressional velocity mean relative error below 3% while the shear velocity mean relative error reaches 75% for the first layer. Incidentally, we note that, among the six parameters to be estimated, the shear velocity of the first layer is the one that has the least influence on the acoustic field at the given frequency of 100 Hz (see Fig. 1), i.e., it is the most difficult to retrieve. However, the poor result for the shear velocity estimate could be partially overcome while maintaining the same computational effort by reducing the search interval at the 10th and 20th iteration (Fig. 9). In this case the mean relative error is decreased to 1% or less for the compressional velocities and to less than 40% for the shear velocity of the first layer, and less than 5% for the shear velocity of the last layer. The price paid for the improved result is that any interval reduction criteria introduces a potential risk of missing the true parameter value.

3.3. *Genetic algorithms versus RBF based inversion*

The purpose of this section is to evaluate the results of the GA inversion with respect to other global inversion methods. To this aim, we have decided to compare, on the same physical situation, the adaptive GA described in the previous section with a "neural network-like" inversion scheme based on the idea of global approximation of the inverse function with a series of Radial Basis Functions (RBF). The RBF method does *not* belong to the class of global search strategies (as, for instance, simulated annealing), that tend to exhibit the same merits and drawbacks of GA, and for this reason it has been selected as a challenging comparison for the GA.

A complete description of the RBF-based inversion is beyond the scope of the present paper, and the interested reader is referred to Ref. 21. For our purpose here, it is sufficient to say that the RBF method relies on the idea of determining an approximation of the inverse function in the form of a series expansion, where the basis functions take the form of gaussian or gaussian-like functions. The coefficients of the series expansion are determined from a set of known input-output relations ("training set"), generated, for instance, through forward model computations. In the present situation, the "input" is the acoustic field measured on the towed array, and the ouput is the corresponding vector of seafloor parameters. If the training set is generated in such a way to cover most of the significant physical situations, the resulting series expansion will be a smooth approximation of the nonlinear inverse function on its global domain. The computational burden of the RBF method is mainly in the generation of the training set, while the computation of the solution from the measured data can be performed, once the series coefficients are identified, in real time.

It is not straightforward to compare the results of the GA-based and of the RBF-based inversion. For instance, RBF approximations must be evaluated in terms of ensemble errors over a set of cases ("test set") spread over the whole seafloor parameters domain, since we want to test the approximating abilities on the large, and not just locally. On the other hand, GA are evaluated in terms of independent runs on the same data set. Keeping this difference in mind, we report here the results obtained with the RBF inversion. A training set of 800 input-output cases has been generated, by randomly selecting the bottom parameters in an interval equal to the search interval set for the GA, and the series coefficients have been identified. Another set of 50 cases (not included in the training set) has been generated, and the acoustic field has been fed to the RBF expansion, which generated the corresponding seafloor parameters. As in the GA case, the seafloor parameters of interest are the compressional and the shear velocities in the first three seafloor layers.

In Fig. 10, we report the relative error obtained with the RBF method for each case in the test set, and the mean relative error. It can be seen that the mean error in compressional velocity retrieval varies between 1 and 3% (depending on the layer), while the shear velocity mean error is of the order of 20–25% for all layers, with a couple of cases that exhibit very significant deviation from the mean. The presence of these "outliers" in the RBF results are generally an indication of inadequacies in the training set.

Apart from the outliers, if one compare these results with those of Fig. 9, one can see that the two methods yield qualitatively similar results, with a slightly better performance of GA with respect to compressional velocity and the third layer shear velocity, and a moderate preference towards RBF for the first layer shear velocity. In terms of computational burden, the RBF method required 800 runs of forward models, while the GA run required 1800 runs, i.e., there is a factor of about two between the two approaches.

It is important to remark that, with this example, we are not trying to establish which is the "best" method for seafloor parameters identification, but what kind of results and approximation is reasonable to expect in the given experimental configuration, i.e., with a moderate aperture towed array in shallow water at a given frequency (100 Hz in this case). Moreover, work is still in progress to improve the performance of both the adaptive GA and the RBF-based scheme.

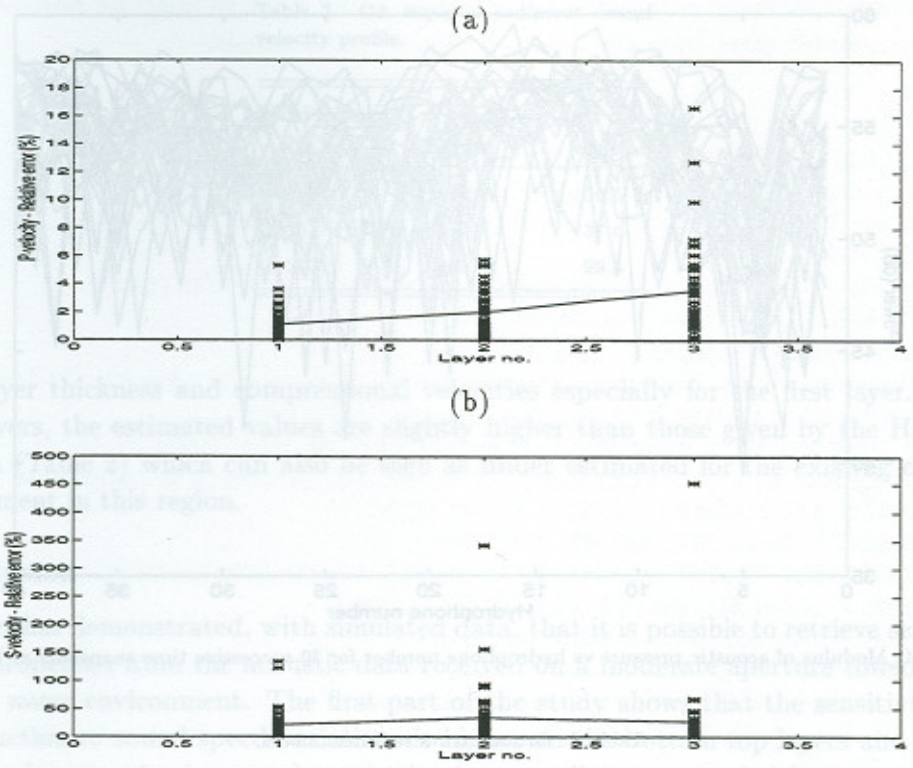

Fig. 10. Relative errors in P-velocity (a) and S-velocity (b). Each $*$ represents the result of a single run and the solid line is the mean relative error computed over 50 independent runs.

4. Real Data Inversion

4.1. *Sea trial and ground truth measurements*

In this section genetic algorithm-based methods were applied to the inversion of field data. The data set of interest was recorded during the sea trial SAG1-94, in the Panteleria Bank, Strait of Sicily, and consisted of 5 minutes of data starting at 10:48 am on the 4th of March 1994. During this run, R/V ALLIANCE was towing both a 156 m aperture horizontal array and a sound source. The array was composed of 40 hydrophones at 4 m spacing and was at approximately 50 m depth. The source was at 40 m depth and the range between the source and the first array hydrophone (closest to the ship) was 535 m. The source was emiting continuous tones at 125 Hz. The environment was characterized by an almost isovelocity sound speed profile at 1508 m/s in the 120 m depth water column over a layered sub-bottom. Figure 11 shows a series of 30 successive time snapshots taken during that experiment. Independent ground truth measurements were carried out during the cruise including sparker surveys, bottom sampling and geophone data transmission[22] revealing a bottom geoacoustic model structure as given in Table 2. Note that, only part of the information of Table 2, the two upper layers, was actually measured during the cruise, the deeper layers in particular, were derived from Hamilton's regression curves based on historical knowledge of the region.

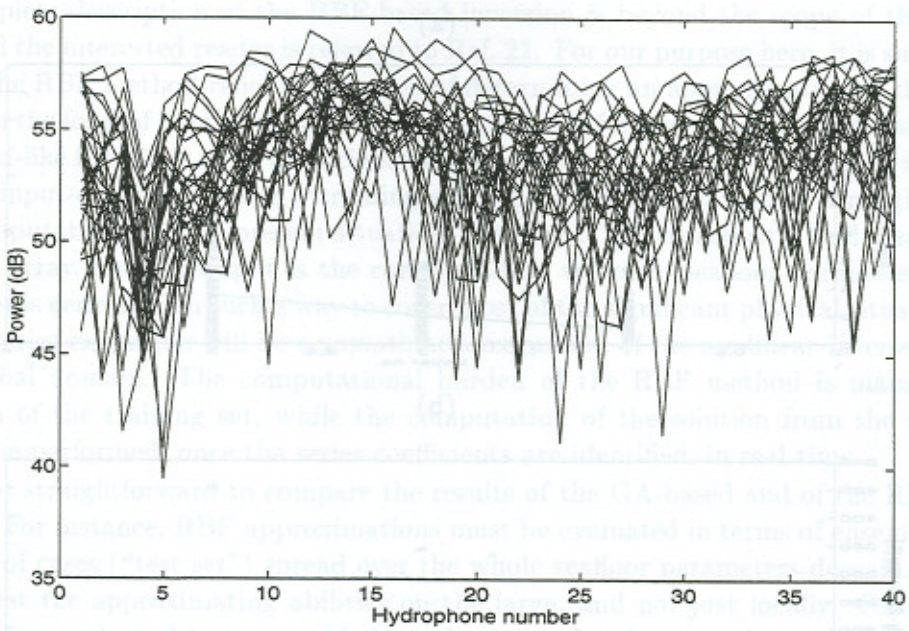

Fig. 11. Modulus of acoustic pressure vs hydrophone number for 30 successive time snapshots at 125 Hz.

Table 2. Ground truth sediment model.

Thickness (m)	P vel. (m/s)	S vel. (m/s)
6.0	1550	230.0
8.0	1585	275.0
18.0	1610	290.0
≥ 18.0	1700	360.0

4.2. *GA data inversion*

The genetic algorithm code was run with a population size of 24 samples and a total number of forward model runs of 1500. The objective function chosen is the conventional matched-filter of Eq. (3). For the purpose of the inversion, a hard basement characterized by a P-velocity of 2200 m/s and a S-velocity $\geq$ 900 m/s was placed below the third layer. The inversion was carried out on the data shown in Fig. 11 in two steps. First, a single snapshot inversion was attempted for the P-velocity and layer thicknesses while keeping constant all the other system and environmental parameters. Second, using the estimated layer thicknesses the inversion was made for all other pings and the results are shown in Table 3.

The standard deviations shown in Table 3 were estimated from the successive inversions of 30 time pings, each of them worth approximately 3 secs of data. It can be noted that, there is a fairly good agreement between the true and the estimated parameters, both

Table 3. GA inverted sediment sound velocity profile.

Thickness (m)	P vel. (m/s)	Std. dev. (m/s)
6.0	1590	50.5
16.0	1649	37.6
26.0	1800	99.5

for the layer thickness and compressional velocities especially for the first layer. For the deeper layers, the estimated values are slightly higher than those given by the Hamilton's regression (Table 2) which can also be seen as under estimated for the existing carbonate sand sediment in this region.

5. Conclusion

This paper has demonstrated, with simulated data, that it is possible to retrieve sea bottom physical properties from the acoustic data received on a moderate aperture towed array in a shallow water environment. The first part of the study shows that the sensitivity of the object function to sound speed variations is higher on the bottom top layers and increases with array length. An increased sensitivity is generally accompanied by a cost function nonmonotonic behavior creating local extrema and making it hazardous to reach the global optimum. Density and attenuations (both compressional and shear) have in general small influence on the acoustic field structure and are therefore difficult to estimate. Increasing the signal-frequency bandwidth by incoherent module averaging has no significant influence on sensitivity. A cost function relying on the conventional matched filter has shown low sensitivity to sensor noise and has been extended to match directional data from bottom arrivals at several frequencies. A technique for providing a maximum likelihood broadband estimate of the peak location has been derived and showed a good performance at high SNR. Mismatch cases, mainly those related to array/source relative position, showed that deviations of more than $\lambda/5$ in depth and $\lambda/3$ in range may give erroneous extremum location and therefore biased final estimates. The second part of the paper deals with the inversion of the acoustic data using a modified genetic algorithm. It is shown that allowing the variation of the search interval along iterations provided a more accurate final estimate. In our study, a maximum-likelihood based estimator is proposed and in a two-parameter case, it showed to be able to more rapidly converge to the global optimum than the conventional matched-filter estimator. In the simultaneous 6 parameters case at 10 dB SNR, the estimates obtained were within 1% of the true values for compressional velocities, while the accuracy of the shear velocities estimate strongly depends, as one may expect, on the sensitivity of the acoustic field to these parameters. Comparison of the adaptive GA performance with an inversion scheme based on RBF series expansion yield substantially similar results. Finally, it has been shown with field data that it is indeed possible to

retrieve detailed sediment compressional velocities using a 156 m aperture horizontal array within a reasonable error from the assumed ground truth values.

References

1. W. H. Munk and C. Wunsch, *Deep Sea Res.* **A26**, 123 (1979).
2. B. Cornuelle, C. Wunsch, D. Behringer, T. Birdsall, M. Brown, R. Heinmiller, R. Knox, K. Metzger, W. Munk, J. Spiesberger, R. Spindel, D. Webb, and P. Worcester, *J. Phys. Ocean* **15**, 133 (1985).
3. B. Cornuelle, W. Munk, and P. Worcester, *J. Geophys. Res.* **94**, 6232 (1989).
4. H. P. Bucker, *J. Acous. Soc. Am.* **59**, 368 (1976).
5. R. Klemm, *Signal Processing* **3**, 333 (1981).
6. A. B. Baggeroer, W. A. Kuperman, and H. Schmidt, *J. Acous. Soc. Am.* **83**, 571 (1988).
7. J. F. Smith and S. Finette, *J. Acous. Soc. Am.* **94**, 2315 (1993).
8. J. Q. D. Tran and W. S. Hodgkiss, *J. Acous. Soc. Am.* **94**, 2851 (1993).
9. A. B. Baggeroer and W. A. Kuperman, "Matched field processing in underwater acoustics," *Proc. NATO ASI*, Madeira (Portugal), 83–122 (1992).
10. S. D. Rajan, *J. Acous. Soc. Am.* **92**, 2126 (1992).
11. M. D. Collins and W. A. Kuperman, *J. Acous. Soc. Am.* **92**, 2770 (1992).
12. A. Turgut, *J. Acous Soc. Am.* **93**, Pt. 2, 2aAO15 (1993).
13. P. Gerstoft, *J. Acous. Soc. Am.* **95**, 770 (1994).
14. W. A. Kuperman, M. D. Collins, and H. Schmidt "A fast simulated annealing algorithm for the inversion of marine sediment seismo-acoustic parameters," in *Shear Waves in Marine Sediments*, eds. J. M. Hovem, M. D. Richardson, and R. D. Stoll (Kluwer, Dordtrecht, Holland, 1991), pp. 521–528.
15. P. Gerstoft and A. Caiti, "Acoustic estimation of bottom parameters: error bounds by local global methods," *Proc. 2nd European Conf. in Underwater Acoustics*, ed. L. Bjorno, Copenhagen, DK, 1994.
16. J. F. Lynch, S. D. Rajan, and G. V. Frisk, *J. Acous. Soc. Am.* **89**, 648 (1991).
17. G. V. Frisk, "Inverse methods in ocean bottom acoustic," in *Oceanographic and Geophysical Tomography*, eds. Y. Desaubies, A. Tarantola, and J. Zinn-Justin (Elsevier, 1990).
18. H. Schmidt, "SAFARI: Seismo-acoustic fast field algorithm for range independent environments," La Spezia, Italy, SACLANTCEN SR-113 (1988).
19. S. Jesus, "A sensitivity study for full-field inversion of geo-acoustic data with a towed array in shallow water," in *Proc. of Sec. European Coference on Underwater Acoustics*, ed. L. Bjorno (European Commission, Copenhagen, 1994), pp. 899–904.
20. D. E. Goldberg, *Genetic Algorithms in Search, Optimization and Machine Learning* (Addison-Wesley, 1988).
21. A. Caiti, T. Parisini and R. Zoppoli, "Seafloor parameters estimation: approximating the inverse map through RBF networks," in *Full-field Inversion Methods in Ocean and Seismic Acoustics*, eds. O. Diachok, A. Caiti, P. Gerstoft, H. Schmidt (Kluwer, to be published in Spring 1995).
22. A. Caiti, T. Akal and R. D. Stoll, *IEEE J. Oceanic Engi.* **19**, 58 (1994).